# Longitudinal preclinical magnetic resonance imaging of diffuse tumor burden in intramedullary myeloma following bortezomib therapy

**Deep K Hathi**[1,2], **John A. Engelbach**[2], **Jens Hillengass**[3], **Deborah Veis**[4], **Samuel Achilefu**[1,2,5,6], **Joel R. Garbow**[2,6], **Monica Shokeen**[1,2,6,*]

[1]Department of Biomedical Engineering, Washington University in St. Louis, St. Louis, Missouri, United States of America 63110

[2]Department of Radiology, Washington University School of Medicine, St. Louis, Missouri, United States of America 63110

[3]Department of Oncology, Roswell Park Comprehensive Cancer Institute, Buffalo, New York, United States of America 14203

[4]Department of Pathology and Immunology, Washington University School of Medicine, St. Louis, Missouri, United States of America 63110

[5]Department of Biochemistry and Biophysics, Washington University School of Medicine, St. Louis, Missouri, United States of America 63110

[6]Alvin J. Siteman Cancer Center at Washington University School of Medicine and Barnes Jewish Hospital, St. Louis, Missouri, United States of America 63110

## Abstract

Multiple myeloma (MM) is a largely incurable, debilitating hematologic malignancy of terminally differentiated plasma cells in the bone marrow (BM). Identification of therapeutic response is critical for improving outcomes and minimizing costs and off-target toxicities. To assess changes in BM environmental factors and therapy efficacy, there is a need for noninvasive, nonionizing, longitudinal, preclinical methods. Here, we demonstrate the feasibility of preclinical magnetic resonance imaging (MRI) for longitudinal imaging of diffuse tumor burden in a syngeneic, immunocompetent model of intramedullary MM. C57Bl/KaLwRij mice were implanted intravenously with 5TGM1-GFP tumors and treated with a proteasome inhibitor, bortezomib, or vehicle control. MRI was performed weekly with a Helmholtz radiofrequency coil placed on the hind leg. Mean normalized T1-weighted signal intensities and T2 relaxation times were quantified for each animal following manual delineation of BM regions in the femur and tibia. Finally, tumor burden was quantified for each tissue using hematoxylin and eosin staining. Changes in T2 relaxation times correlated strongly to cell density and overall tumor burden in the BM. Median T2 relaxation times and regional T1-weighted contrast uptake were shown to be most relevant in identifying post-therapy disease stage in this model of intramedullary MM. In summary, our

---

[*]**Corresponding Author:** Dr. Monica Shokeen, 4515 McKinley Ave RM 2216, St. Louis, MO 63110, 314-362-8979, mshokeen@wustl.edu.

results highlighted potential preclinical MRI markers for assessing tumor burden and BM heterogeneity following bortezomib therapy, and demonstrated the application of longitudinal imaging with preclinical MRI in an immunocompetent, intramedullary setting.

## Graphical Abstract:

There is a scarcity of preclinical MRI studies of bone marrow malignancies. Here, we demonstrate multi-parametric MRI to longitudinally follow changes in the bone marrow in response to multiple myeloma stage and therapy in a preclinical immunocompetent model. The key findings in the intramedullary model were that T1-weighted contrast-enhanced MRI and T2 relaxation times are indicative of spatiotemporal disease progression and response to proteasome inhibitor therapy. Histology of the bone marrow validated the MR observations.
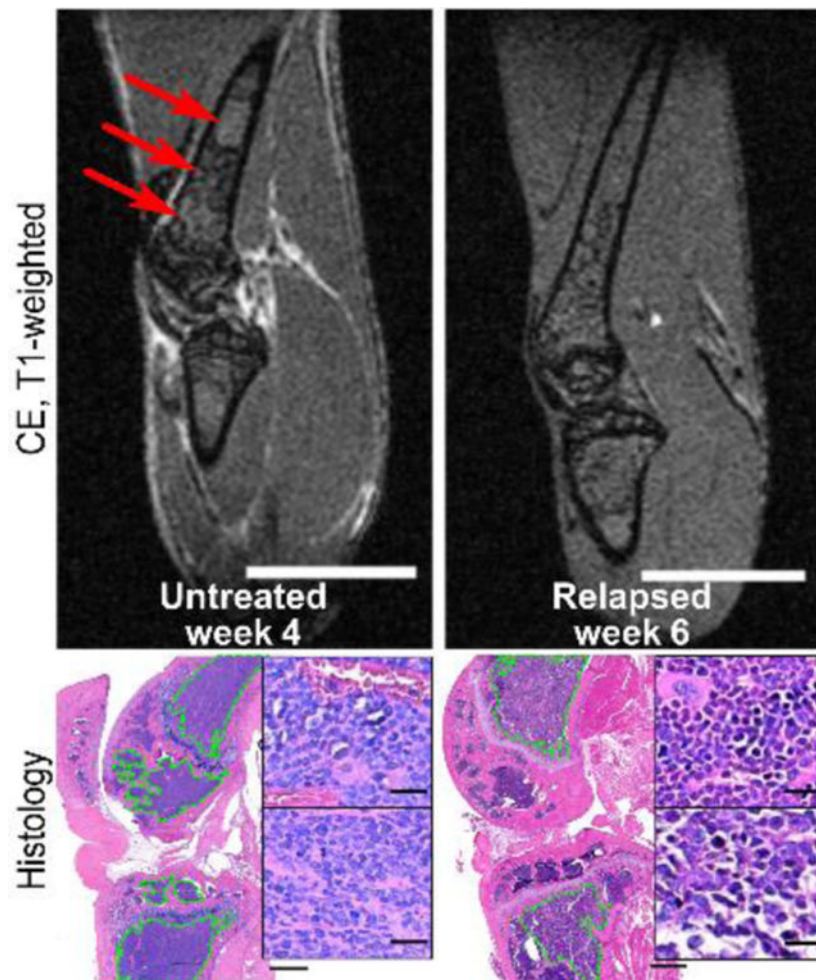


## Keywords

preclinical MRI; diffuse tumor burden; intramedullary multiple myeloma (MM); bortezomib treatment response; longitudinal imaging

## Introduction

Multiple myeloma (MM) is a cancer of terminally differentiated plasma B-cells in the bone marrow (BM) that accounts for approximately 15% of all mortalities associated with hematologic malignancies[1,2]. Despite recent improvements in MM treatment, the efficacy of MM therapeutic strategies is still variable, especially at the late stages of cancer progression[3]. Changes in therapy efficacy are influenced, in part, by the interactions of myeloma cells with the BM microenvironment. As a result, imaging strategies to noninvasively assess changes in the BM microenvironment can provide valuable information for treatment stratification.

In MM, clinical magnetic resonance imaging (MRI) is used extensively to delineate lesions and stage disease progression following treatment[4]. Traditional biological markers, including bone remodeling and angiogenesis-related factors and plasma cell infiltration, are correlated to the observed lesions in T1-weighted, non-contrast enhanced and fat-suppressed, T2-weighted MRI[5,6]. In particular, diffuse and variegated BM lesions have been identified with heterogeneous signal in T1-weighted imaging, with high correlation between level of diffuse infiltration and poor prognosis[5]. Additional MR techniques, including diffusion-weighted imaging, dynamic contrast-enhanced imaging, and magnetic resonance spectroscopy have also highlighted significant differences in diffusion coefficients, vascularity, and adipose tissue fraction between responders and non-responders[7–9].

While the role of MRI is well established in the clinic, studies demonstrating the potential of preclinical MRI in MM are scarce. Due to its excellent soft-tissue contrast and resolution, MRI provides a preclinical platform for studying the BM microenvironment in a noninvasive, nonionizing, longitudinal manner. Here, we demonstrate the use of multi-parametric MRI for longitudinal imaging of the tumor burden in the BM in a syngeneic immunocompetent model of intramedullary diffuse MM. Treatment with a proteasome inhibitor, bortezomib, was performed, due to its relevance in MM clinical care at all stages and its effect on BM remodeling[10]. Effective changes in tissue heterogeneity and tumor burden from T1-weighted imaging and T2 parametric maps, respectively, were correlated with histology for validation. T2 relaxation times and regional T1-weighted contrast uptake were shown to be most relevant for identifying post-therapy disease stage in this model of intramedullary MM.

## Experimental

### Cell Culture and Reagents

5TGM1-GFP cells (5TGM1; kind gift from Dr. K. N. Weilbaecher, Washington University, Department of Medicine) were maintained at $10^6$ cells/mL in Iscove's Modified Dulbecco Medium supplemented with 10% v/v fetal bovine serum and 1% penicillin/streptomycin (all from Thermo Fisher Scientific, MA, USA). Bortezomib (Sigma Aldrich, MO, USA) doses were prepared prior to each therapy injection.

### Tumor model and bortezomib therapy

All animal studies were conducted according to protocols approved by the Washington University Institutional Animal Care and Use Committee. Mice were anesthetized under 2% v/v isoflurane/100% $O_2$ prior to tumor implantation. Female 4–8 week old C57Bl/KaLwRij mice were injected intravenously with $10^6$ 5TGM1 cells, *via* the lateral tail vein, which resulted in diffuse tumor burden in the BM and spleen[11].

Tumor-bearing mice were separated into randomly assigned untreated (n=5) and bortezomib-treated (n=9) independent cohorts (Figure 1). Bortezomib therapy was administered intraperitoneally at 1 mg/kg twice a week beginning on day 14 post tumor implantation[12]. Untreated animals received the vehicle control on the same schedule. Non-tumor bearing animals (n=4) were imaged once.

### Preclinical Magnetic Resonance Imaging

Preclinical ^{1}H MRI experiments were performed on a 4.7-T Agilent/Varian (Santa Clara, CA, USA) DirectDrive MRI scanner employing a horizontal Oxford Instruments (Abington, Oxfordshire, UK) magnet with 40-cm clear bore diameter and an actively shielded Resonance Research Inc. (Billerica, MA) gradient/shim coil assembly of 11.5-cm bore diameter driven by Oy International Electric Company (IEC; Helsinki, Finland) model A-240 amplifiers (~70 gauss/cm is achievable with a rise time of ~120 μs). All imaging experiments were conducted under 1% v/v isoflurane/100% $O_2$ anesthesia. Mice were placed prone, with the hind leg immobilized within a tuned Helmholtz radiofrequency coil. The hind leg was used to image changes in large BM sites with minimal motion artifacts. Body temperature was maintained with an external air heater. Planning and localization of femur and tibia regions of interest (ROIs) were performed using sagittal (field of view (FOV) $2.5\times2.5\times0.5$ cm$^3$) and transverse (FOV $1.5\times1.5\times1.0$ cm$^3$) T1-weighted gradient echo sequences (flip angle 20°, repetition time (TR) 100 ms, echo time (TE) 5 ms). Following field shimming, T2 parametric maps were collected using multi-slice, multiple spin echo (FOV $2\times2\times0.3$ cm$^3$, TR 2s, 7.1 ms $\leq$ TE $\leq$ 113.5 ms, 16 echoes, $0.156\times0.156\times1$ mm$^3$ voxel dimensions, $128\times128\times3$ matrix dimensions, 1 average). Mice were then injected intraperitoneally with 12 μmol MultiHance (Bracco Diagnostics, NJ, USA). To allow the contrast agent to accumulate and approach steady state, CE T1-weighted gradient echo 3D images were collected 8–10 minutes following injection of the agent (FOV $2\times1\times1$ cm$^3$, flip angle 20°, TR 25 ms, TE 4.2 ms, $0.78\times0.78\times0.78$ mm$^3$ voxel dimensions, $128\times256\times128$ matrix dimensions, 4 averages).

### Bone histology and imaging

Following euthanasia, femur and tibia were removed and decalcified. Bone tissue was embedded in paraffin, sectioned at 5 μm thickness, and stained with hematoxylin and eosin (H&E). Brightfield images of the H&E stained slides were acquired using the NanoZoomer Digital Pathology System (NanoZoomer 2.0-HT, Hamamatsu, Japan).

### Data analysis

Image analysis was performed using in-house routines developed on MATLAB R2014b (Mathworks, MA, USA). ROIs for the femur, tibia, and muscle volumes were drawn on each

slice of T1-weighted, non-CE and CE images using ImageJ (National Institutes of Health, MD, USA). To minimize variability in inter-scan T1-weighted image intensity resulting from unavoidable modest variability in coil placement and subject positioning, CE T1-weighted images were normalized by the mean voxel intensity of the muscle volume of interest (VOI). T2 parametric maps were generated using non-linear least squares fitting of the equation $S(t) = A + B \times \exp(-t/C)$ for each voxel, where $S(t)$ is the signal intensity, $t$ is TE, $A$ and $B$ are scaling constants, and $C$ is the voxel-specific T2. The constant, $A$, accounts for both the positive, non-zero mean of Rician noise and any steady-state, non-zero transverse magnetization resulting from imperfect, slice-selective 180° refocusing pulses.

The spatial distribution of T1-weighted signal within the femur and tibia VOIs was assessed by calculating the coefficient of variation of the normalized T1-weighted intensity and textural autocorrelation. To calculate textural autocorrelation, image histograms were distributed into equally sized integer bins and voxels were relabeled to the integer values of their respective bins. A gray-level co-occurrence matrix (GLCM) was computed on the VOI covering each neighboring voxel in 3D space[13,14]. Autocorrelation was calculated as $\sum_i^{N_g} \sum_j^{N_g} p_i p_j$, where $N_g$ and $p$ are the number of gray levels in the scaled image and the GLCM, respectively. Bone histology images were imported into MATLAB using ImageJ and the Bio-Formats application interface[15]. Images were first manually segmented into femur and tibia BM ROIs, and then into tumor and non-tumor ROIs. Tumor burden (%) was calculated for tumor-bearing groups as (Total ROI area – Non-tumor area)/(Total ROI area) * 100%.

### Statistical analysis

Statistical analysis on histogram and texture statistics from the imaging and histology was performed using GraphPad Prism 7.0 (GraphPad, CA, USA). One-way analysis of variance (ANOVA) with Tukey multiple comparisons test was used to assess statistical significance between multiple treatment groups for femur and tibia VOI individually. A $p$-value less than 0.05 was defined as statistically significant. Correlations between MR and histology features were calculated using the Spearman rho coefficient. Finally, to distinguish between pre- and post-therapy time points, a 150-tree random forest was trained on a group of T1-weighted and T2 histogram and heterogeneity features[16]. The features used in this analysis were the median, variance, coefficient of variation, and entropy from femur and tibia VOIs in the T1-weighted images and T2 parametric maps. Classification error was computed as the rate of misclassification against a random one-third of the data at each iteration, while the importance of each feature was computed by dividing misclassification probability by the standard deviation from all trees.

## Results

### Observed differences in normalized 3D CE T1-weighted MRI

Diffuse tumor burden in the femur and tibia VOIs in treated and untreated C57Bl/KaLwRij mice bearing intramedullary 5TGM1 tumors was visualized using normalized CE T1-weighted imaging (Figure 2). Due to heterogeneity in the BM composition of the femur and

tibia, end-stage untreated mice displayed spatial variation in T1-weighted CE image intensity in the femur, and to a lesser extent, tibia (Figure 2B). By contrast, non-tumor bearing (Figure 2A) and end-stage treated (Figure 2C) groups showed minimal spatial heterogeneity in either femur or tibia. Mid-stage, untreated (week 3) and treated (week 4) mice had similar spatial distributions in both femur and tibia (Supplemental Figure 1A–B). Textural analysis of these images confirmed the observed spatial distributions. The GLCM autocorrelation, which measures the fineness of the textured image, was significantly reduced in the femurs of untreated tumor-bearing mice ($p < 0.05$) relative to the non-tumor bearing and treated tumor-bearing groups (Figure 2D). Furthermore, there was a statistically significant increase in the difference in autocorrelation between the treatment time points and the pre-treatment baseline relative to the untreated groups ($p < 0.01$) (Figure 2E).

Statistical analysis of mean T1-weighted CE normalized intensities supported the spatial heterogeneity observations in representative sections (Figure 3A). End-stage (weeks 5–6), treated tumor-bearing mice showed a statistically significant increase in T1-weighted intensity relative to the mid-stage (weeks 3–4) treated and untreated groups in the tibia ($p < 0.01$). Interestingly, in the femur, the mean T1-weighted intensity in the non-tumor bearing group was significantly higher ($p < 0.001$) than in the rest of the groups and had a tighter intra-group distribution relative to the non-tumor tibia VOI. To minimize the underlying intra-animal heterogeneity, the %difference between the pre-treatment and the latter stage time-points was calculated. The end-stage treated group showed a statistically significant increase in the %difference in T1-weighted intensity relative to the mid-stage treated and untreated groups in the tibia ($p < 0.05$), but not the femur (Figure 3B). These results demonstrate that region-specific permeability and contrast agent uptake *via* vascular availability are affected by bortezomib treatment response and tumor burden.

### Effect of disease stage and bortezomib therapy on T2 parametric maps

To identify the effect of treatment on tumor burden, T2 parametric maps were generated. These maps identified substantive changes in the tibia VOI after tumor implantation. The non-tumor-bearing tibia had low overall T2 (Figure 4A), while untreated and treated cohorts displayed similar T2 distributions in both VOIs (Figure 4B, 4C). Interestingly, treated mid- and end-stage animals showed increasing clustering of high T2 values (>45 ms) near the epiphyseal plate (Supplemental Figure 1D).

These observations were further supported by quantitative analysis of the T2 parametric maps (Figure 5A). In both femur and tibia, mean T2 times in the end-stage (weeks 5–6), treated tumor-bearing group was significantly increased relative to the T2 times in the mid-stage treated group ($p < 0.01$). In both VOIs, the non-tumor bearing group had low mean T2, although as observed, the non-tumor T2 in the tibia was significantly lower than in the other groups ($p < 0.001$). Following normalization with pre-treatment imaging, the treated end-stage and mid-stage groups were more heterogeneous in the tibia VOI than in the femur (Figure 5B). In the tibia, there was a statistically significant difference in the %T2 difference between the untreated groups and the end-stage treated group ($p < 0.01$). By contrast, in the femur, there was a significant reduction in the %T2 difference mid-stage treated relative to

the end-stage untreated and treated groups ($p<0.05$). These results suggest that the T2 parametric maps are responsive to the overall disease stage following treatment.

Finally, histogram and heterogeneity features from T1-weighted images and T2 parametric maps were used to identify disease stage post-treatment with a 150-tree random forest. First order descriptive statistics, especially median T2 times, were highlighted as the most predictive features of pre- and post-treatment stage (Supplemental Figure 2A). Using the highest performing features, the intra-class separation area under the receiver operator characteristic curve was greater than 0.79, with total 65% accuracy in classification (Supplemental Figure 2B, 2C). Scaling the data onto a lower dimensional space showed that mid-stage (week 3–4) and end-stage (week 5–6) treated cohorts have similar MR characteristics (Supplemental Figure 2D). This observation suggests that imaging in this animal model can differentiate between pre- and post-therapy conditions, but is less sensitive to changes between the early and late stages of the post-treatment disease progression. In summary, T1-weighted CE imaging and T2 parametric maps were indicative of tumor burden, with significant effects seen in the end-stage, treated, tumor-bearing group.

### Validation of imaging results with H&E of femur and tibia BM

To validate MRI results, the femur and tibia were extracted at end-stage disease and stained with H&E. Non-tumor bearing mice had high lipid content clustered near the femur epiphyseal plate and low overall cell density (Figure 6A). In the end-stage, untreated tumor-bearing group, the healthy BM was overtaken by densely packed, mononuclear tumor cells, while non-tumor BM tissue was sequestered in the epiphysis of the femur and tibia (Figure 6B, Supplemental Figure 3B). Following treatment, tumor tissue was primarily concentrated proximal to the epiphyseal plate in both femur and tibia (Figure 6C, Supplemental Figure 3A). Additionally, both mid- and end-stage, treated groups showed statistically significant reductions in tumor burden in both femur and tibia relative to the untreated mice (Figure 6C, Supplemental Figure 3B). These1`1` results suggest that bortezomib therapy restricts tumor cell growth to the rapidly growing epiphyseal plate region, which may correlate with the observed high T2 values near the epiphyseal plate in some of the animals in the end-stage treated group (Figure 4C).

In summary, histology and tumor burden quantification demonstrated the difference in the distribution of tumor between the untreated and treated tumor-bearing groups. BM in the femur and tibia of untreated animals was dominated completely by tumor tissue, while tumor burden was concentrated proximal to the epiphyseal plate in the treated animals, especially in end-stage, treated disease. The heterogeneity in cell density was positively correlated with the coefficient of variation of the femur and tibia VOIs in the T1-weighted images and T2 parametric maps (Supplemental Figure 4).

## Discussion

This study marks one of the first instances utilizing multi-parametric MRI to longitudinally follow changes in the BM in response to MM stage and therapy in a preclinical immunocompetent model. Previously, Fryer *et al* demonstrated that a combination of *in vivo* bioluminescence and T2-weighted tumor volume were correlated to therapy response in an

intratibial immunocompromised model of MM[17]. Similarly, Gauvain *et al* used a metastatic melanoma model in immunocompetent C57Bl/6 mice to identify early stage bone metastases using a combination of T2-weighted and T2 parametric imaging[18]. In both studies, the tumor model resulted in focal lesions, which have well-defined boundaries. However, in this study, a diffuse intramedullary tumor model was generated by intravenous injection of syngeneic tumor cells within an immunocompetent strain. The advantages of this model include the preservation of the immune response to the myeloma cells and the presence of therapy-induced inflammation. Since MRI offers high soft-tissue contrast and spatial resolution, we hypothesized that MRI could provide a noninvasive, longitudinal approach for studying changes in the BM induced by bortezomib therapy and MM disease progression. The key MR features and their corresponding biological correlates in the BM are summarized in Table 1.

T1-weighted, CE, 3D MRI signal intensities were indicative of contrast uptake within regions of tissue. Gadolinium-based contrast agents induce shortening of T1 relaxation times, resulting in increases in T1-weighted signal intensity in highly vascular and permeable regions relative to necrotic and less vascularized regions[19]. Spatial heterogeneity was quantitatively assessed using textural autocorrelation, which is correlated to the textural coarseness of the image. Image coarseness decreases with increasing MR signal homogeneity that can arise from reduced tumor burden, uniform contrast distribution, or a combination of the two factors within the VOI. The uptake of contrast within the BM in the femur and tibia was spatially heterogeneous, especially in the end-stage, untreated, tumor-bearing animals. By contrast, treatment with bortezomib resulted in increases in homogenous contrast agent uptake within the BM in both femur and tibia. Bortezomib causes significant marrow remodeling, resulting in reduction in osteoclast activity and cytokine secretion, and inhibition of tumor-induced angiogenesis[20,21]. At the same time, healing and tumor cell death induced by bortezomib may also generate increased inflammation, which may result in an increase in contrast uptake within high tumor burden regions after relapse. By contrast, in the mid-stage treated group, bortezomib efficacy and inhibition of neo-vascularization likely dominates, resulting in low normalized T1-weighted intensity.

In contrast to T1-weighted CE images, T2 parametric maps were reflective of tumor burden and increased regional water content. There was less spatial heterogeneity in the T2 parametric maps, although this observation may have partially resulted from the reduced resolution in the T2 maps compared to the T1-weighted 3D images. T2 values were highest in both treated and untreated mice near the epiphyseal plate. This may be caused by the high tumor burden in those regions due to the presence of hematopoietic niches in the epiphysis and the availability of tumor-promoting cellular and extracellular matrix factors. Interestingly, mean T2 relaxation time was significantly increased in the tibia of the tumor-bearing groups relative to the non-tumor bearing group. The increase in T2 relaxation from the non-tumor group compared to the tumor-bearing groups was not as exaggerated in the femur. These trends may be a function of the underlying composition of the femur and tibia in the C57Bl/KaLwRij model. There is higher hematopoietic and cellular content in the femur BM, with the tibial BM, especially in the distal tibia, dominated by adipose tissue[22]. In the presence of myeloma, T2 relaxation times increased, although interestingly, the

relative difference in T2 relaxation was higher in the treated animals than in the untreated groups. These results suggest that T2 relaxation is indicative of overall tumor burden and post-treatment disease progression.

Histology with H&E staining was used to validate the MRI observations. Tumor burden in the end-stage untreated animals completely displaced normal BM in the femur and tibia. This result approximates advanced MM in humans, with homogeneous, packed diffuse infiltration dominating the BM[23]. The lack of marrow adipose tissue in the tumor-bearing animals may be partly due to the age of the mice, since significant changes in marrow adipocyte depositions occur in older animals. The study used young, 4–6 week old mice, since young animals have high rates of bone remodeling and higher plasticity in the marrow composition. Both mid-treatment and end-stage cohorts had reduced tumor burden, which was concentrated proximal to the epiphyseal plate. Increases in the normalized T1-weighted intensity and T2 relaxation times were observed at the epiphyseal plate. Additionally, the overall heterogeneity in cell density correlated with heterogeneity in the T1-weighted and T2 parametric imaging in the femur and tibia. These correlations and observations suggest that the MR results are reflective of the changes in the BM environment following bortezomib therapy.

The main limitations of this study are the rapid disease kinetics and the absence of validation with a focal lesion model and a non-tumor bearing, treated control cohort. Due to the aggressive nature of this tumor model, animals treated with bortezomib transitioned rapidly from mid-stage to end-stage disease, leaving subtle changes in the BM. Classification of disease stage following therapy using random forests indicated that T1-weighted contrast uptake and T2 relaxation times were very similar at all post-therapy time points. Furthermore, contrast uptake and changes in the spatial distribution of signal intensities were affected by the underlying heterogeneity in the distribution of hematopoietic and fatty marrow in the BM. Comparison with a well-circumscribed, focal lesion model may further validate the observations of this study and minimize the effect of spatiotemporal heterogeneity on the imaging results, especially at early and mid-stage disease. Finally, the addition of a non-tumor cohort with bortezomib treatment may provide a useful control for therapy-induced inflammation.

In conclusion, this study demonstrates that T1-weighted CE MRI and T2 relaxation times are indicative of disease progression and response to bortezomib therapy in an immunocompetent intramedullary model of MM. As such, it marks the first instance of using MRI to longitudinally study the behavior of the BM in the preclinical model with diffuse MM infiltration, showing significant histogram and textural feature correlation to tumor burden in the presence of myeloma therapy. The study also highlighted potential preclinical MRI markers for assessing changes to the BM induced by MM and therapy. Future studies will include MR spectroscopy to assess changes in adipose tissue composition in response to myeloma in both young and old mice, the use of alternate hypo-proliferative myeloma cell lines, and testing with combination therapies and newer proteasome inhibitors.

## Supplementary Material

Refer to Web version on PubMed Central for supplementary material.

## Acknowledgments

## Abbreviations:

| | |
|---|---|
| **MM** | Multiple myeloma |
| **BM** | Bone marrow |
| **CE** | Contrast-enhanced |
| **GFP** | Green fluorescent protein |
| **GLCM** | Gray-level co-occurrence matrix |
| **ANOVA** | Analysis of variance |
| **VOI** | Volume of interest |
| **H&E** | Hematoxylin and eosin |

## References

1. Becker N Epidemiology of multiple myeloma In: Moehler T, Goldschmidt H, eds. Multiple Myeloma. Berlin, Heidelberg: Springer Berlin Heidelberg; 2011:25–35.

2. Palumbo A, Anderson K. Multiple myeloma. New England Journal of Medicine. 2011;364(11): 1046–1060. [PubMed: 21410373]

3. Brenner H, Gondos A, Pulte D. Recent major improvement in long-term survival of younger patients with multiple myeloma. Blood. 2008;111(5):2521–2526. [PubMed: 17901246]

4. Rajkumar SV, Dimopoulos MA, Palumbo A, Blade J, Merlini G, Mateos M-V, Kumar S, Hillengass J, Kastritis E, Richardson P, Landgren O, Paiva B, Dispenzieri A, Weiss B, LeLeu X, Zweegman S, Lonial S, Rosinol L, Zamagni E, Jagannath S, Sezer O, Kristinsson SY, Caers J, Usmani SZ, Lahuerta JJ, Johnsen HE, Beksac M, Cavo M, Goldschmidt H, Terpos E, Kyle RA, Anderson KC, Durie BGM, Miguel JFS. International Myeloma Working Group updated criteria for the diagnosis of multiple myeloma. Lancet Oncol. 2014;15(12):e538–e548. [PubMed: 25439696]

5. Moulopoulos LA, Dimopoulos MA, Christoulas D, Kastritis E, Anagnostou D, Koureas A, Roussou M, Gavriatopoulou M, Migkou M, Iakovaki M, Gkotzamanidou M, Tasidou A, Terpos E. Diffuse MRI marrow pattern correlates with increased angiogenesis, advanced disease features and poor prognosis in newly diagnosed myeloma treated with novel agents. Leukemia. 2010;24(6):1206–1212. [PubMed: 20428203]

6. Lee S-Y, Kim H-J, Shin YR, Park H-J, Lee Y-G, Oh SJ. Prognostic significance of focal lesions and diffuse infiltration on MRI for multiple myeloma: a meta-analysis. Eur Radiol. 2017;27(6):2333–2347. [PubMed: 27595836]

7. Hillengass J, Bauerle T, Bartl R, Andrulis M, McClanahan F, Laun FB, Zechmann CM, Shah R, Wagner-Gund B, Simon D, Heiss C, Neben K, Ho AD, Schlemmer HP, Goldschmidt H, Delorme S, Stieltjes B. Diffusion-weighted imaging for non-invasive and quantitative monitoring of bone marrow infiltration in patients with monoclonal plasma cell disease: a comparative study with histology. Br J Haematol. 2011;153(6):721–728. [PubMed: 21517815]

8. Nosàs-Garcia S, Moehler T, Wasser K, Kiessling F, Bartl R, Zuna I, Hillengass J, Goldschmidt H, Kauczor H-U, Delorme S. Dynamic contrast-enhanced MRI for assessing the disease activity of multiple myeloma: a comparative study with histology and clinical markers. J Magn Reson Imaging. 2005;22(1):154–162. [PubMed: 15971177]

9. Oriol A, Valverde D, Capellades J, Cabanas ME, Ribera JM, Arus C. In vivo quantification of response to treatment in patients with multiple myeloma by 1H magnetic resonance spectroscopy of bone marrow. MAGMA. 2007;20(2):93–101. [PubMed: 17410391]

10. Mitsiades CS, Mitsiades NS, Munshi NC, Richardson PG, Anderson KC. The role of the bone microenvironment in the pathophysiology and therapeutic management of multiple myeloma: interplay of growth factors, their receptors and stromal interactions. Eur J Cancer. 2006;42(11):1564–1573. [PubMed: 16765041]

11. Soodgupta D, Zhou H, Beaino W, Lu L, Rettig M, Snee M, Skeath J, DiPersio JF, Akers WJ, Laforest R, Anderson CJ, Tomasson MH, Shokeen M. Ex Vivo and In Vivo Evaluation of Overexpressed VLA-4 in Multiple Myeloma Using LLP2A Imaging Agents. J Nucl Med. 2016;57(4):640–645. [PubMed: 26742713]

12. Hurchla M, Garcia-Gomez A, Hornick M, Ocio E, Li A, Blanco F, Collins L, Kirk C, Piwnica-Worms D, Vij R, Tomasson M, Pandiella A, San Miguel J, Garayoa M, Weilbaecher K. The epoxyketone-based proteasome inhibitors carfilzomib and orally bioavailable oprozomib have anti-resorptive and bone-anabolic activity in addition to anti-myeloma effects. Leukemia. 2013;27:430–440. [PubMed: 22763387]

13. van Griethuysen JJM, Fedorov A, Parmar C, Hosny A, Aucoin N, Narayan V, Beets-Tan RGH, Fillion-Robin J-C, Pieper S, Aerts HJWL. Computational Radiomics System to Decode the Radiographic Phenotype. Cancer Res. 2017;77(21):e104–e107. [PubMed: 29092951]

14. Haralick RM, Shanmugam K, Dinstein I. Textural Features for Image Classification. IEEE Transactions on Systems, Man, and Cybernetics. 1973;SMC-3(6):610–621.

15. Linkert M, Rueden CT, Allan C, Burel J-M, Moore W, Patterson A, Loranger B, Moore J, Neves C, MacDonald D, Tarkowska A, Sticco C, Hill E, Rossner M, Eliceiri KW, Swedlow JR. Metadata matters: access to image data in the real world. The Journal of Cell Biology. 2010;189(5):777–782. [PubMed: 20513764]

16. Breiman L Random Forests. Machine Learning. 2001;45(1):5–32.

17. Fryer RA, Graham TJ, Smith EM, Walker-Samuel S, Morgan GJ, Robinson SP, Davies FE. Characterization of a novel mouse model of multiple myeloma and its use in preclinical therapeutic assessment. PLoS One. 2013;8(2):e57641. [PubMed: 23437401]

18. Gauvain KM, Garbow JR, Song S-K, Hirbe AC, Weilbaecher K. MRI detection of early bone metastases in b16 mouse melanoma models. Clin Exp Metastasis. 2005;22(5):403–411. [PubMed: 16283483]

19. Tokuda O, Hayashi N, Matsunaga N. MRI of bone tumors: Fast STIR imaging as a substitute for T1-weighted contrast-enhanced fat-suppressed spin-echo imaging. J Magn Reson Imaging. 2004;19(4):475–481. [PubMed: 15065172]

20. Zangari M, Suva LJ. The effects of proteasome inhibitors on bone remodeling in multiple myeloma. Bone. 2016;86:131–138. [PubMed: 26947893]

21. Caravita T, de Fabritiis P, Palumbo A, Amadori S, Boccadoro M. Bortezomib: efficacy comparisons in solid tumors and hematologic malignancies. Nat Clin Pract Oncol. 2006;3(7):374–387. [PubMed: 16826218]

22. Bartelt A, Koehne T, Tödter K, Reimer R, Müller B, Behler-Janbeck F, Heeren J, Scheja L, Niemeier A. Quantification of Bone Fatty Acid Metabolism and Its Regulation by Adipocyte Lipoprotein Lipase. Int J Mol Sci. 2017;18(6):1264.

23. Bartl R, Frisch B, Burkhardt R, Fatehmoghadam A, Mahl G, Gierster P, Sund M, Kettner G. Bone-Marrow Histology in Myeloma - Its Importance in Diagnosis, Prognosis, Classification and Staging. Br J Haematol. 1982;51(3):361–375. [PubMed: 7104223]
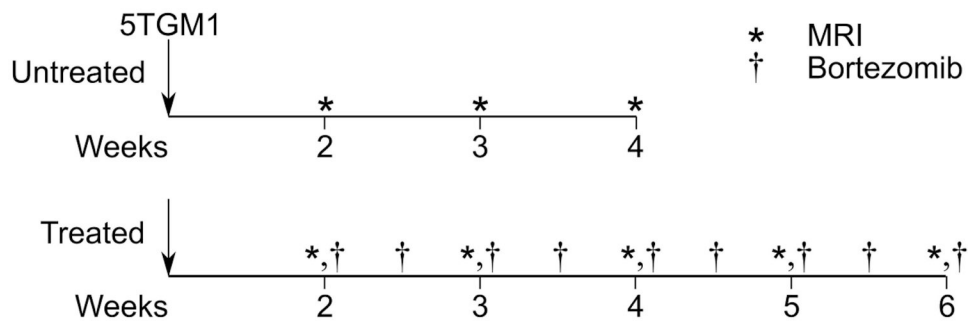
**Figure 1:**

Study design, imaging, and therapy timeline. Untreated tumor-bearing (N = 5) 5TGM1/ KaLwRij were imaged weekly with non-CE T2 parametric mapping and 3D CE T1-weighted MR weekly beginning two weeks post 5TGM1 tumor implantation. Untreated animals were euthanized at the onset of systemic paralysis, which occurred approximately four weeks post tumor implantation. The bortezomib treatment cohort (N = 9) was similarly implanted with 5TGM1 tumors and injected with bortezomib via intraperitoneal injection at 1 mg/kg twice a week, beginning two weeks post tumor implantation. On imaging days (e.g., day 14, 21, 28), therapy and vehicle injections were performed immediately following imaging. As with the untreated tumor-bearing cohort, each mouse was imaged weekly with non-CE T2 parametric mapping and a 3D CE T1-weighted pulse sequence.
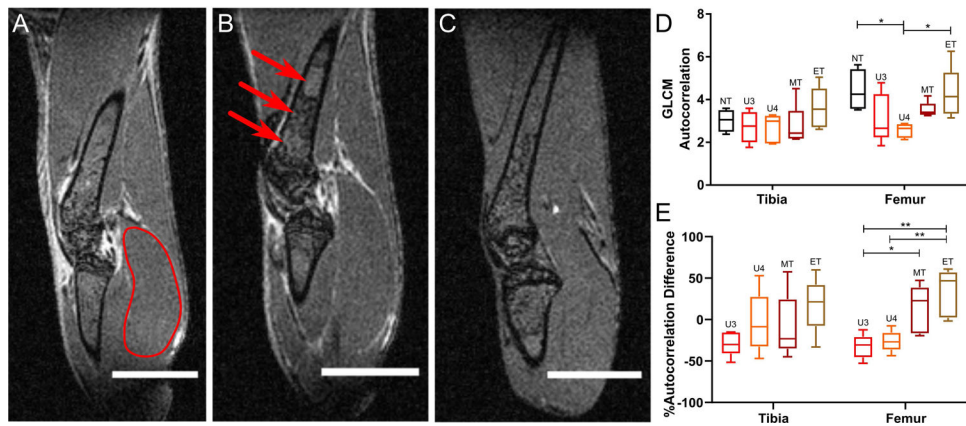
**Figure 2:**
Representative T1-weighted CE-MRI. Each voxel in the volume was normalized by the mean of representative muscle VOI located in the lower leg. (A) Non-tumor bearing. Red outline indicates reference muscle ROI used for normalization. (B) Untreated tumor-bearing, week 4. (C) Treated tumor-bearing, week 6. Red arrows highlight regions of significant spatial intensity variation. Scale bar, 4 mm. (D) Mean gray-level co-occurrence matrix (GLCM) autocorrelation in normalized tibia and femur VOIs in non-tumor (NT), untreated tumor-bearing at weeks 3 (U3) and 4 (U4), and treated tumor-bearing groups at weeks 3–4 (MT) and weeks 5–6 (ET). (E) Mean GLCM autocorrelation relative to week 2 baseline for each animal (%difference = (Time-point Mean – Baseline Mean)/(Baseline Mean)). Statistical significance was assessed using a one-way ANOVA with Tukey multiple comparisons test performed individually on the tibia and femur VOIs ($*p < 0.05$). Whiskers indicate 5–95% confidence intervals.
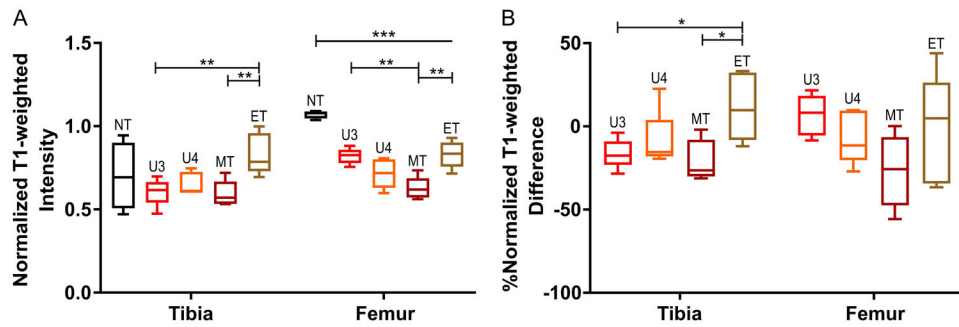
**Figure 3:**

Mean CE T1-weighted intensity, normalized by mean muscle intensity, in femur and tibia VOIs. (A) Mean CE T1-weighted normalized intensity in non-tumor bearing (NT) mice, untreated tumor bearing mice at weeks 3 (U3) and 4 (U4), and treated tumor-bearing mice at weeks 3–4 (MT) and 5–6 (ET). (B) Mean CE, T1-weighted normalized intensity relative to week 2 baseline for each animal (%difference = (Time-point Mean – Baseline Mean)/(Baseline Mean)). Statistical significance was calculated using a one-way ANOVA with the Tukey multiple comparisons test performed individually on the tibia and femur VOIs (*$p < 0.05$, **$p < 0.01$, ***$p < 0.001$; closed line indicates comparison between two groups, open-ended line indicates statistical significance between one group against all other included groups). Whiskers indicate 5–95% confidence intervals.
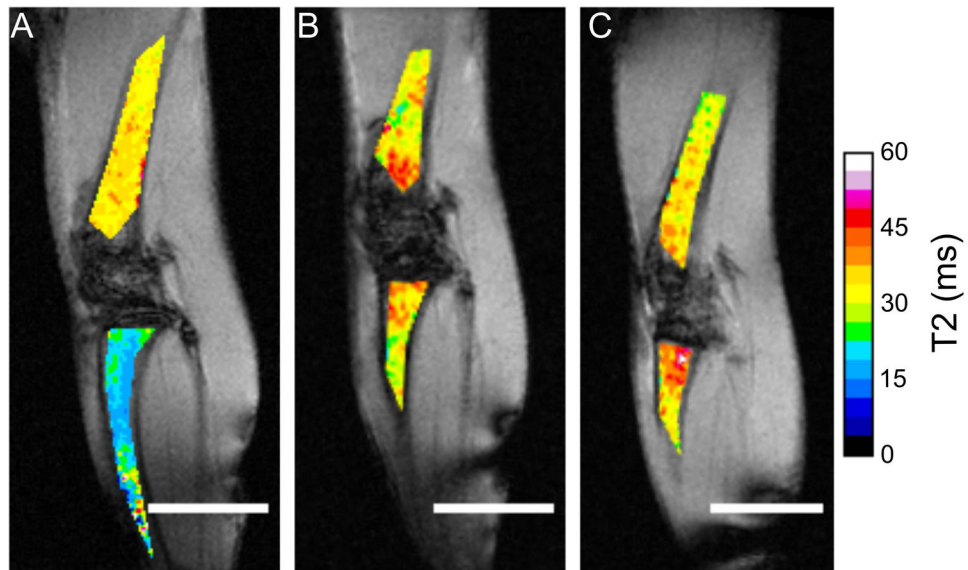
**Figure 4:**
Representative T2 parametric maps of femur and tibia BM. (A) Non-tumor bearing mice. (B) Untreated tumor-bearing mice, week 4. (C) Treated tumor-bearing mice, week 6. Femur and tibia T2 maps were overlaid on non-CE, oblique, T1-weighted intensity images normalized by the mean voxel intensity of the muscle ROI. Scale bar, 4 mm; T2 range 0–60 ms.
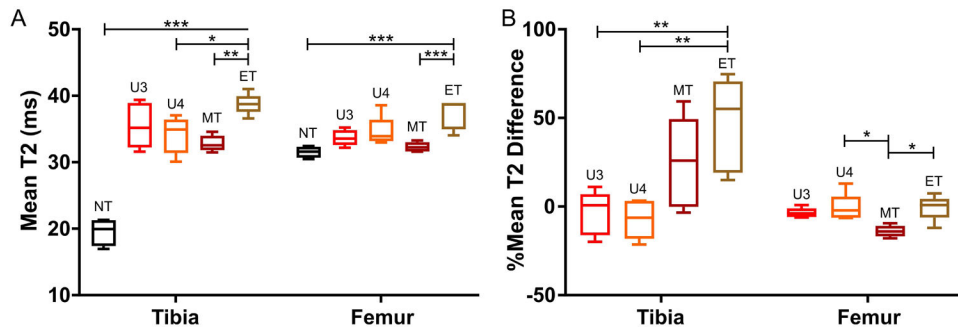
**Figure 5:**
Mean T2 in femur and tibia VOIs. (A) Mean T2 in non-tumor bearing (NT) mice, untreated tumor-bearing mice at weeks 3 (U3) and 4 (U4), and treated tumor-bearing mice at weeks 3–4 (MT) and weeks 5–6 (ET). (B) Mean T2 relative to week 2 baseline for each animal (%difference = (Time-point Mean – Baseline Mean)/(Baseline Mean)). Statistical significance was assessed using a one-way ANOVA with Tukey multiple comparisons test performed individually on the tibia and femur VOIs ($*p < 0.05$, $**p < 0.01$, $***p < 0.001$; closed line indicates comparison between two groups, open-ended line indicates statistical significance between one group against all other included groups). Whiskers indicate 5–95% confidence intervals.
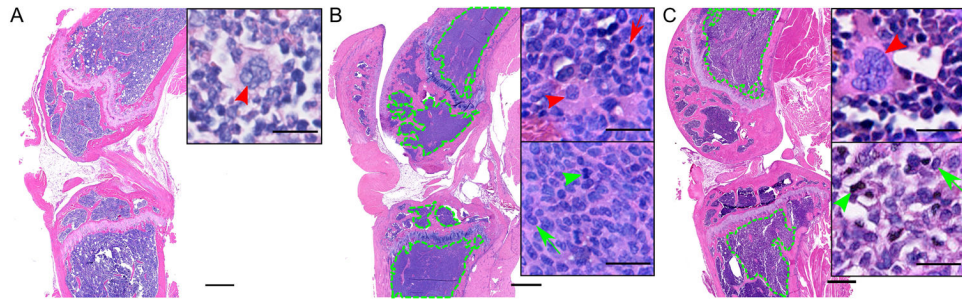
**Figure 6:**
Representative H&E sections. (A) Non-tumor bearing mice. (B) Untreated tumor-bearing mice, week 4. (C) Treated tumor-bearing mice, week 6. Green outline indicates tumor boundaries. Top inset highlights non-tumor cells, as indicated by the presence of large, cytoplasm-rich, multi-nucleated megakaryocytes (red arrowhead) and lobular, concave nuclei (red arrow). The bottom inset highlights tumor cells, as indicated by the presence of segmented, chromatin-rich mitoses (green arrowhead) and oval plasma cell nuclei (green arrow). Scale bar, 500 μm; inset scale bar, 20 μm.

**Table 1:**

Summary of MR markers and their corresponding biological features for each imaging group relative to the untreated week 4 group. 0, no effect; +, difference in features; ++, statistically significant difference in features.

| | | | Untreated | | Treated | |
|---|---|---|---|---|---|---|
| **MR marker** | **Biological Correlate** | **Non-tumor** | **Week 3** | **Week 4** | **Mid-stage (Wks 3–4)** | **End-stage (Wks 5–6)** |
| Autocorrelation and normalized T1-weighted intensity | Tissue Homogeneity | ++ | 0 | 0 | + | ++ |
| Mean T2 relaxation times | Tumor burden | N/A | 0 | 0 | + | ++ |
| H&E cell density | Total tumor burden | N/A | N/A | 0 | ++ | ++ |